Numer. Math. (2004) 97: 397–425
Digital Object Identifier (DOI) 10.1007/s00211-003-0506-5

Numerische Mathematik

Residual-based a posteriori error estimate for hypersingular equation on surfaces

Dedicated to W. L. Wendland on the occasion of his 65th birthday

Carsten Carstensen[1], **M. Maischak**[2], **D. Praetorius**[1], **E.P. Stephan**[2]

[1] Institute for Applied Mathematics and Numerical Analysis, Vienna University of Technology, Wiedner Hauptstrasse 8-10/115, 1040 Wien, Austria;
e-mail: {Carsten.Carstensen, Dirk.Praetorius}@tuwien.ac.at
[2] Institut für Angewandte Mathematik, Universität Hannover, Welfengarten 1, 30167 Hannover, Germany;
e-mail: {maischak, stephan}@ifam.uni-hannover.de

Received June 18, 2001 / Revised version received May 21, 2002 /
Published online February 4, 2004 –

Summary. The hypersingular integral equation of the first kind equivalently describes screen and Neumann problems on an open surface piece. The paper establishes a computable upper error bound for its Galerkin approximation and so motivates adaptive mesh refining algorithms. Numerical experiments for triangular elements on a screen provide empirical evidence of the superiority of adapted over uniform mesh-refining. The numerical realisation requires the evaluation of the hypersingular integral operator at a source point; this and other details on the algorithm are included.

Mathematics Subject Classification (1991): 65N30, 65R20, 73C50

1 Introduction

Let Ω be a bounded domain in $\mathbb{R}^3$ with Lipschitz boundary $\partial\Omega$ and let $\Gamma \subset \partial\Omega$ be an open surface. Neumann screen problems on Γ in three dimensions yield the hypersingular integral equation,

(1.1)
$$Wu(x) := -\frac{1}{2\pi}\,\frac{\partial}{\partial n_x}\int_\Gamma \Big(\frac{\partial}{\partial n_y}\,\frac{1}{|x-y|}\Big)\,u(y)\,ds_y = f(x) \quad \text{for any } x \in \Gamma$$

Correspondence to: C. Carstensen

with the hypersingular operator $W : \widetilde{H}^s(\Gamma) \to H^{s-1}(\Gamma)$ for $0 < s < 1$. With Theorem 4.2, this paper establishes the residual-based a posteriori error estimate

$$\| u - u_h \|_{\widetilde{H}^s(\Gamma)} \leq c_1 \| h_{\mathcal{T}}^{1-s} R \|_{L^2(\Gamma)} \tag{1.2}$$

for the Galerkin approximation u_h to the exact solution u with respect to a triangulation $\mathcal{T}$ of Γ with mesh size $h_{\mathcal{T}}$ and its residual $R := f - Wu_h \in L^2(\Gamma)$. (The fractional order Sobolev spaces $H^s(\Gamma)$, $\widetilde{H}^s(\Gamma)$, $H^{-s}(\Gamma)$, $\widetilde{H}^{-s}(\Gamma)$ will be defined in Section 2.)

Similar estimates in two dimensions are proved by a reduction to an estimate for the single-layer potential by simple integration along the curve [C2, CS]. Hence, in three dimensions, a new technique is required. In contrast to the former work [CS, C2, CMS] the interpolation estimate (c.f., e.g., Equation (2.6) below) cannot be employed. Instead of a localization inequality (in Lemma 2.1), we use the reversed version of Lemma 2.3.

Inequality (1.2) ensures the reliability of the a posteriori error bound. The reverse inequality, which ensures the efficiency, is an open problem as the technique in [C1] requires a closed boundary.

The numerical validation of (1.2) and numerical evidence on the efficiency are the experimental contributions of this paper. Two algorithms generate effective meshes in two screen examples and provide empirical evidence for the superiority of adaptive over uniform mesh-refining.

The remaining part of the paper is organized as follows. Preliminaries on non-local Sobolev spaces of fractional order follow in Section 2. Those on the mesh geometry are collected in Section 3. The main result (1.2) is proved in Section 4. A comparison with a multilevel error estimator is given in Theorem 5.2 of Section 5. The computation of the refinement indicator

$$\eta_T := h_T^{1/2} \| R \|_{L^2(T)} \quad \text{for } T \in \mathcal{T}$$

via a quadrature rule requires the pointwise evaluation of $R(x)$. This calculation is described in Section 6. The implementation of a Galerkin boundary element method, based on (conforming) triangles on Γ is documented in Section 7. There, two adaptive algorithms (A_R) and (A_H) are proposed and run for two examples.

2 Preliminaries on interpolation spaces

Let Ω be a bounded Lipschitz domain in $\mathbb{R}^3$ with (closed) boundary

$$\widehat{\Gamma} = \partial\Omega \quad \text{and} \quad \Gamma \subset \widehat{\Gamma} \tag{2.1}$$

an (relatively) open surface piece. We provide a partition

$$\mathcal{T} = \{\Gamma_1, \ldots, \Gamma_n\} \tag{2.2}$$

of Γ into elements $\Gamma_1, \ldots, \Gamma_n$ supposed to be closed (flat) triangles or parallelograms in $\mathbb{R}^3$.

For any (relatively) open set $\omega \subseteq \widehat{\Gamma}$ and $0 \leq s \leq 1$, we define Sobolev spaces of fractional order by interpolation

$$\widetilde{H}^s(\omega) := [L^2(\omega); H_0^1(\omega)]_s \quad \text{and} \quad H^s(\omega) := [L^2(\omega); H^1(\omega)]_s, \tag{2.3}$$

where $[X_0; X_1]_s$ denotes the complex (L^2-) interpolation of X_0 and $X_1 \subseteq X_0$ [BL], [L]. The norm $\| \cdot \|_{H^1(\omega)}$ in $H^1(\omega)$ is given by the surface gradient ∇ as $\| f \|^2_{H^1(\omega)} = \| f \|^2_{L^2(\omega)} + \| \nabla f \|^2_{L^2(\omega)}$ and $H_0^1(\omega)$ is the completion of $\{f \in \mathrm{Lip}(\omega) : f = 0 \text{ on } \partial\omega\}$ in $H^1(\omega)$. We define the dual spaces

$$H^{-s}(\omega) := \big(\widetilde{H}^s(\omega)\big)^* \qquad \text{and} \qquad \widetilde{H}^{-s}(\omega) := \big(H^s(\omega)\big)^* \tag{2.4}$$

and extend the scalar product in $L^2(\omega)$ to the duality pairing

$$\langle \cdot; \cdot \rangle \quad \text{in } \widetilde{H}^{-s}(\omega) \text{ and } H^s(\omega). \tag{2.5}$$

We remark the following interpolation properties.

Remark 2.1. Let X_0, X_1 being normed spaces with $X_1 \subseteq X_0$ and $X := [X_0; X_1]_s$ the complex interpolation ($0 \leq s \leq 1$). For the norm of X holds the estimate

$$\| \cdot \|_{[X_0;X_1]_s} \leq \| \cdot \|^{1-s}_{X_0} \, \| \cdot \|^s_{X_1} \tag{2.6}$$

but we stress that it is not needed below. Further, let $Y := [Y_0; Y_1]_s$ being the complex interpolation of two normed spaces Y_0, Y_1 with $Y_1 \subseteq Y_0$. If $T \in L(X_0, Y_0)$ can also be viewed as $T \in L(X_1, Y_1)$ then $T : X \to Y$ is well-defined and continuous as well with operator norm

$$\| T \|_{L(X,Y)} \leq \| T \|^{1-s}_{L(X_0,Y_0)} \| T \|^s_{L(X_1,Y_1)}. \tag{2.7}$$

The following two lemmas from [P,SS] are frequently employed in the literature.

Lemma 2.1 ([P,SS]). *If $f \in \widetilde{H}^s(\Gamma)$ with $f|_{\Gamma_j} \in \widetilde{H}^s(\Gamma_j)$ for all $j = 1, \ldots, n$, then*

$$\| f \|^2_{\widetilde{H}^s(\Gamma)} \leq \sum_{j=1}^{n} \| f|_{\Gamma_j} \|^2_{\widetilde{H}^s(\Gamma_j)}. \qquad \square \tag{2.8}$$

Lemma 2.2 ([P,SS]). *If $f \in H^s(\Gamma)$, then $f|_{\Gamma_j} \in H^s(\Gamma_j)$ for all $j = 1, \ldots, n$ with*

$$\sum_{j=1}^{n} \| f|_{\Gamma_j} \|^2_{H^s(\Gamma_j)} \leq \| f \|^2_{H^s(\Gamma)}. \qquad \square \tag{2.9}$$

Remarks 2.2. (i) The lemmas hold for all $s \in \mathbb{R}$ if we interpret the restriction correctly.

(ii) The constant factor 1 on the right-hand sides in the lemmas (not displayed explicitly) holds for complex interpolation and needs to be replaced by n-independent constants in case of real interpolation and alternative definitions by extension or by Sobolev-Slobodeckij norms.

(iii) The assumption $f|_{\Gamma_j} \in \widetilde{H}^s(\Gamma_j)$ may be neglected in Lemma 2.1 if we understand $\| f|_{\Gamma_j} \|_{\widetilde{H}^s(\Gamma_j)} = \infty$ in case $f|_{\Gamma_j} \notin \widetilde{H}^s(\Gamma_j)$.

Lemma 2.1 was employed for localization in almost all residual-based a posteriori error estimates for integral equations of the first kind. Here, we utilize the following Lemma 2.3, a derivation of Lemma 2.2. Let γ be the relative boundary of Γ on $\widehat{\Gamma}$. Define $H^1_D(\omega) := \{f \in H^1(\omega) : f = 0 \text{ on } \gamma \cap \partial\omega\}$ for an open subset $\omega \subseteq \Gamma$ and consider for $0 \leq s \leq 1$

$$H^s_D(\omega) := [L^2(\omega); H^1_D(\omega)]_s \tag{2.10}$$

Lemma 2.3. *If $f \in \widetilde{H}^s(\Gamma)$ then $f|_{\Gamma_j} \in H^s_D(\Gamma_j)$ for all $j = 1, \ldots, n$, and*

$$\sum_{j=1}^{n} \| f \|^2_{H^s_D(\Gamma_j)} \leq \| f \|^2_{\widetilde{H}^s(\Gamma)} \tag{2.11}$$

Proof. The essential observation is that the product of interpolated spaces is the interpolation of the products (even with equal norms [BL]), i.e.,

$$\prod_{j\in J} \underbrace{[X_0^j; X_1^j]_s}_{=:X_s^j} \equiv \Big[\prod_{j\in J} X_0^j ; \prod_{j\in J} X_1^j \Big]_s =: X_s$$

With $X_s^j = [L^2(\Gamma_j); H^1_D(\Gamma_j)]_s = H^s_D(\Gamma_j)$, this shows

$$\sum_{j=1}^{n} \| u|_{\Gamma_j} \|^2_{H^s_D(\Gamma_j)} = \| (u|_{\Gamma_j} : j = 1, \ldots, n) \|^2_{X_s}. \tag{2.12}$$

For $s = 0$ and $s = 1$, the linear mapping

$$T_s : \widetilde{H}^s(\Gamma) \to X_s ; \quad u \mapsto (u|_{\Gamma_j} : j = 1, \ldots, n) \tag{2.13}$$

is bounded with norm ≤ 1. Interpolation yields that T_s is well-defined with $\|T_s\| \leq 1$ for all $0 \leq s \leq 1$ and hence

$$\| (u|_{\Gamma_j} \,:\, j = 1, \ldots, n) \|_{X_s}^2 \leq \|u\|_{\widetilde{H}^s(\Gamma)}^2. \tag{2.14}$$

Combining (2.12)-(2.14) we deduce (2.11) and, in particular, we show that the restriction $(\cdot)|_{\Gamma_j} : \widetilde{H}^2(\Gamma) \to H_D^s(\Gamma_j)$ is a well-defined bounded linear operator. □

3 Preliminaries of finite element approximation

Each element Γ_j of the triangulation $\mathcal{T}$ is supposed to be a closed (flat) triangle or parallelogram in $\mathbb{R}^3$. Hence, we can define nodal local basis functions which are linear combinations of $1, x, y$ (for Γ_j a triangle) or $1, x, y, xy$ (for Γ_j a parallelogram) on the (two-dimensional) reference element $\Gamma_{ref} = \text{conv}\{(0,0), (1,0), (0,1)\}$ resp. $\Gamma_{ref} = [0,1]^2$. Although Γ is the open surface of a polyhedragonal closed boundary $\widehat{\Gamma} = \partial\Omega$, the concept of a regular triangulation applies to $\mathcal{T} = \{\Gamma_1, \ldots, \Gamma_n\}$ as well: Two distinct and intersecting Γ_j and Γ_k share either an entire edge or a vertex. The relative boundary γ of Γ on $\widehat{\Gamma}$ is a finite union of closed polygons which consists of entire edges.

The set of all nodes in the triangulation is denoted by $\mathcal{N}$ and the free nodes by $\mathcal{K} := \mathcal{N} \setminus \gamma$. The set of all edges in the triangulation is denoted by $\mathcal{E}$ and $\mathcal{E}$ is split into edges on the boundary γ, namely $\mathcal{E}_\gamma := \{E \in \mathcal{E} \,:\, E \subseteq \gamma\}$, and interior edges $\mathcal{E}_\Gamma := \{E \in \mathcal{E} \,:\, E \not\subseteq \gamma\}$.

For each free node $z \in \mathcal{K}$ there is a hat function φ_z which equals zero on each element Γ_k (if $z \notin \Gamma_k$) or one of the nodal local basis functions (if z is a vertex of Γ_k) such that $\varphi_z(z) = 1$ and $\varphi_z(x) = 0$ for all $x \in \mathcal{N} \setminus \{z\}$. The hat functions are Lipschitz continuous and form a partition of unity. Their linear hull

$$\mathcal{S} := \text{span}\{\varphi_z \,:\, z \in \mathcal{K}\} \subseteq H_0^1(\Gamma) \tag{3.1}$$

satisfies proper boundary conditions. Since $\{\varphi_z \,:\, z \in \mathcal{K}\}$ is, in general, not a partition of unity, we choose a node $\zeta(z) \in \mathcal{K}$ for each $z \in \mathcal{N} \setminus \mathcal{K}$ and define $\zeta(z) = z$ for $z \in \mathcal{K}$. We get a partition of $\mathcal{N}$ into card($\mathcal{K}$) classes $I(z) := \{\tilde{z} \in \mathcal{N} \,:\, \zeta(\tilde{z}) = z\}$, $z \in \mathcal{K}$. For each $z \in \mathcal{K}$ set

$$\psi_z := \sum_{\tilde{z} \in I(z)} \varphi_{\tilde{z}} \tag{3.2}$$

and notice that $\{\psi_z \,:\, z \in \mathcal{K}\}$ is a partition of unity. It is required that

$$\Omega_z := \{x \in \Gamma \,:\, 0 < \psi_z(x)\} \tag{3.3}$$

is connected and contains only a limited number of elements. We remark that $\psi_z \neq \varphi_z$ implies that $\gamma \cap \partial\Omega_z$ has a positive surface measure. Those definitions follow and adapt [CB] in order to employ an approximation operator $(0 \leq s \leq 1)$

$$\mathcal{J} : \widetilde{H}^s(\Gamma) \to \mathcal{S} \subseteq \widetilde{H}^s(\Gamma). \tag{3.4}$$

For each $g \in L^1(\Gamma)$ let $g_z \in \mathbb{R}$ be $g_z := \dfrac{\int_{\Omega_z} g\psi_z \, ds}{\int_{\Omega_z} \varphi_z \, ds}$ for $z \in \mathcal{K}$ and then set

$$\mathcal{J}g := \sum_{z\in\mathcal{K}} g_z \varphi_z \quad \in \mathcal{S}. \tag{3.5}$$

The following approximation properties of $\mathcal{J}$ proved for $\Gamma \subseteq \mathbb{R}^2$ in [CB, Theorem 2.1, Equation (2.10)] hold as well under the present assumptions, where $h_z := \operatorname{diam}(\Omega_z)$, $z \in \mathcal{K}$, denotes the Euclidean diameter of Ω_z.

Lemma 3.1 ([CB]). *There is a constant $c_2 > 0$ that depends on Γ and the aspect ratio of the elements (but not on their sizes) such that for all $z \in \mathcal{K}$ and $g \in H_0^1(\Gamma)$ we have*

$$\| \psi_z g - \varphi_z g_z \|_{L^2(\Omega_z)} \leq c_2 \min\left\{ \| g \|_{L^2(\Omega_z)}, \, h_z \| \nabla g \|_{L^2(\Omega_z)} \right\}. \tag{3.6}$$ □

4 A Posteriori error estimate

Suppose that the residual $R := f - Wu_h = W(u - u_h) \in L^2(\Gamma)$ satisfies the Galerkin conditions

$$\langle R; \varphi_z \rangle = 0 \qquad \text{for all } z \in \mathcal{K}, \tag{4.1}$$

where $\langle \cdot; \cdot \rangle$ denotes the duality pairing on $\widetilde{H}^{-s}$ and H^s, c.f. (2.5). Then we have the following residual-based a posteriori error estimate.

Theorem 4.1. *There is a constant $c_3 > 0$ such that for all $R \in L^2(\Gamma)$ with* (4.1) *and $0 \leq s \leq 1$ there holds*

$$\| R \|_{H^{s-1}(\Gamma)} \leq c_3 \Big(\sum_{z\in\mathcal{K}} h_z^{2-2s} \| R \|^2_{L^2(\Omega_z)} \Big)^{1/2}. \tag{4.2}$$

Proof. Since $(\psi_z : z \in \mathcal{K})$ defines a partition of unity, we have $R = \sum_{z\in\mathcal{K}} \psi_z R$. This combined with (4.1) shows for $g \in H_0^1(\Gamma)$

$$\langle R; g \rangle = \sum_{z\in\mathcal{K}} \langle R; g\psi_z \rangle = \sum_{z\in\mathcal{K}} \langle R; g\psi_z - g_z\varphi_z \rangle \tag{4.3}$$

with $g_z \in \mathbb{R}$ defined as above. For $s = 0$ and $s = 1$ the linear operator

$$T_s : H_D^s(\Omega_z) \to L^2(\Omega_z),\ f \mapsto f\psi_z - f_z\varphi_z \tag{4.4}$$

(where $f_z \in \mathbb{R}$ and Ω_z as above, see (3.3)) is well-defined and continuous with operator norm $\le c_2$ for $s = 0$ and $\le c_2 h_z$ for $s = 1$ according to Lemma 3.1. By interpolation we deduce $\|T_{1-s}\| \le c_2 h_z^{1-s}$, i.e.,

$$\| g\psi_z - g_z\varphi_z \|_{L^2(\Omega_z)} \le c_2 h_z^{1-s} \| g \|_{H_D^{1-s}(\Omega_z)}. \tag{4.5}$$

A Cauchy inequality in (4.3) and the estimate (4.5) show

$$\langle R; g\rangle \le c_2 \Big(\sum_{z\in\mathcal{K}} h_z^{2-2s} \| R \|^2_{L^2(\Omega_z)} \Big)^{1/2} \Big(\sum_{z\in\mathcal{K}} \| g \|^2_{H_D^{1-s}(\Omega_z)} \Big)^{1/2} \tag{4.6}$$

and it remains to prove, with the help of Lemma 2.3, that

$$\sum_{z\in\mathcal{K}} \| g \|^2_{H_D^{1-s}(\Omega_z)} \le c_4 \| g \|^2_{\widetilde{H}^{1-s}(\Gamma)} \tag{4.7}$$

with a constant $c_4 > 0$. A coloring argument (e.g., as in [CMS, Proof of Lemma 3.1]) shows that we can find a finite number of index sets $J_1, J_2, \ldots, J_M$ such that $\{\Omega_z : z \in J_k\}$ are pairwise disjoint for all $j = 1, \ldots, M$. The number M depends on the overlap of the patches $(\Omega_z : z \in \mathcal{K})$ and so on the topology whence on the aspect ratios of the elements (and on Γ). Lemma 2.3 now implies for each set J_k (and Ω_z replacing Γ_j)

$$\sum_{z\in J_k} \| g \|^2_{H_D^{1-s}(\Omega_z)} \le \| g \|^2_{\widetilde{H}^{1-s}(\Gamma)} \qquad \text{for } k = 1, \ldots, M. \tag{4.8}$$

Utilizing this and a finite number of triangle inequalities we prove (4.7). This concludes the proof since $H_0^1(\Gamma)$ is a dense subspace of $\widetilde{H}^{1-s}(\Gamma)$. □

The following main result of this section guarantees reliability of our estimator

$$\eta := \Big(\sum_{T\in\mathcal{T}} \eta_T^2 \Big)^{1/2} \quad \text{with } \eta_T := h_T^{1-s} \| R \|_{L^2(T)} \text{ and}$$
$$h_T := \operatorname{diam}(T) \quad \text{for } T \in \mathcal{T}.$$

Theorem 4.2. *For $0 < s < 1$, there is a constant $c_5 > 0$ that depends on s, Γ, and the aspect ratio of the elements (but not their size) such that*

$$\| u - u_h \|_{\widetilde{H}^s(\Gamma)} \le c_5 c_6 \| h_{\mathcal{T}}^{1-s} R \|_{L^2(\Gamma)}, \tag{4.9}$$

where the $\mathcal{T}$-piecewise constant $h_{\mathcal{T}} \in L^\infty(\Gamma)$ is defined by $h_{\mathcal{T}}(x) = h_T$ for $x \in T$ and $c_6 := \max\{h_z/h_T : z \in \mathcal{K}, T \in \mathcal{T}$ with $T \subseteq \Omega_z\}$.

Proof. The hypersingular operator $W : \widetilde{H}^s(\Gamma) \to H^{s-1}(\Gamma)$ is a continuous, linear bijection (c.f., e.g., [CS] and the references therein). By the open mapping theorem the inverse map W^{-1} is continuous, i.e., $\|W^{-1}\| < \infty$. Since $R = W(u - u_h)$ we obtain

$$\| u - u_h \|_{\widetilde{H}^s(\Gamma)} \leq \|W^{-1}\| \, \| R \|_{H^{s-1}(\Gamma)}. \tag{4.10}$$

Theorem 4.1 and the finite overlap of the $\{\Omega_z : z \in \mathcal{K}\}$ yield

$$\begin{aligned} \| R \|_{H^{s-1}(\Gamma)} &\leq c_3 \Big(\sum_{z \in \mathcal{K}} \| h^{1-s} R \|^2_{L^2(\Omega_z)} \Big)^{1/2} \\ &\leq M c_3 \| h^{1-s} R \|_{L^2(\Gamma)} \leq M c_3 c_6 \| h_{\mathcal{T}}^{1-s} R \|_{L^2(\Gamma)} \end{aligned} \tag{4.11}$$

with $M \in \mathbb{N}$ as in the proof of Theorem 4.1 and $h(x) := \max\{h_z : x \in \Omega_z\}$. □

5 Multilevel error estimation

This section is devoted to a brief description of the multilevel error estimator μ from [MuS, MaS], and a comparison with η. It was already remarked that the hypersingular operator $W : \widetilde{H}^s(\Gamma) \to H^{s-1}(\Gamma)$ is a continuous, linear bijection for $0 < s < 1$. For $s = 1/2$ it defines a continuous and elliptic bilinear form $\langle u; v \rangle_W := \langle Wu; v \rangle$ on $\widetilde{H}^{1/2}(\Gamma)$, whence the induced energy norm $\| u \|_W := \langle u; u \rangle_W^{1/2}$ is an equivalent norm on $\widetilde{H}^{1/2}(\Gamma)$.

In contrast to the previous sections we require at least two meshes where one triangulation $\mathcal{T}_h$ is a refinement of $\mathcal{T}_H$. (Any notation is used in the sense of Section 3 indexed with h resp. H.) The set of free nodes $\mathcal{K}_h$ and $\mathcal{K}_H$ give rise to hat functions $(\varphi_z : z \in \mathcal{K}_h)$ and $(\Phi_z : z \in \mathcal{K}_H)$ with respect to $\mathcal{T}_h$ and $\mathcal{T}_H$, respectively. If $\mathcal{S}_h$ and $\mathcal{S}_H$ denote the respective discrete spaces, $\mathcal{S}_H \subseteq \mathcal{S}_h$ and

$$\mathcal{S}_h = \mathcal{S}_H \oplus \operatorname{span}\{\varphi_z : z \in \mathcal{K}_h \backslash \mathcal{K}_H\}, \tag{5.1}$$

with respective discrete solutions u_h and u_H. For the practical computation, only u_H is required, $\mathcal{S}_h$ plays the role of a fictitious larger space. However, the saturation assumption,

$$\| u - u_h \|_W \leq \kappa \| u - u_H \|_W, \tag{5.2}$$

for some fixed $0 \leq \kappa < 1$, plays an essential role.

Definition 5.1. *For each $z \in \mathcal{K}_h$, let $\mu_z := \langle R; \varphi_z \rangle / \| \varphi_z \|_W$ with $R := f - Wu_H$.*

Theorem 5.1 ([MuS,MaS]). *Under the saturation assumption* (5.2) *we have*

$$c_7 \sum_{z\in\mathcal{K}_h\backslash\mathcal{K}_H} \mu_z^2 \le \| u - u_H \|_W^2 \le c_8 \sum_{z\in\mathcal{K}_h\backslash\mathcal{K}_H} \mu_z^2. \qquad (5.3)$$ □

Remarks 5.2. (i) The constant c_8 in (5.3) depends on $1/(1-\kappa)$ and (possibly) degenerates as $\kappa \to 1$.

(ii) The constant c_7 is robust in $0 \le \kappa < 1$.

(iii) The two-level estimator

$$\mu := \Big(\sum_{z\in\mathcal{K}_h\backslash\mathcal{K}_H} \mu_z^2 \Big)^{1/2} \qquad (5.4)$$

performs very accurately in practice; its justification in (5.3), however, depends crucially on the saturation assumption (5.2).

(iv) In contrast to the finite element context for partial differential equations [D, DN], a proof of (5.2) is unknown for boundary element problems.

Theorem 5.2. *There is an $h_{\mathcal{T}}$-independent constant c_9 such that, for each $z \in \mathcal{K}_h\backslash\mathcal{K}_H$ and* $\operatorname{supp}\varphi_z \subseteq T_1 \cup T_2$ *with $T_1, T_2 \in \mathcal{T}_H$, we have*

$$\mu_z \le c_9 \| h_{\mathcal{T}}^{1/2} R \|_{L^2(T_1\cup T_2)} \le c_9(\eta_{T_1} + \eta_{T_2}). \qquad (5.5)$$

The proof of (5.5) requires the following lemma.

Lemma 5.3. *For each triangulation $\mathcal{T}$ and a corresponding free node $z \in \mathcal{K}$ with hat function φ_z, and $h_z := \operatorname{diam}(\operatorname{supp}\varphi_z)$, we have $\| \varphi_z \|_{\widetilde{H}^s(\Gamma)} \approx h_z^{1-s}$, i.e., there exist positive h_z-independent constants c_{10} and c_{11} such that, for $0 \le s \le 1$,*

$$c_{10} h_z^{1-s} \le \| \varphi_z \|_{\widetilde{H}^s(\Gamma)} \le c_{11} h_z^{1-s}. \qquad (5.6)$$

The constants c_{10}, c_{11} depend on Γ and the shape (not the size) of the elements.

Proof. Throughout this proof we abbreviate $a \le c\, b$ by $a \lesssim b$ and write $a \approx b$ if $a \lesssim b$ and $b \lesssim a$. The involved multiplicative constants do not depend on the mesh-sizes but may depend on Ω, Γ, or the shape of the elements. Direct calculations show the upper estimate in (5.6) for $s = 0$ and $s = 1$. Interpolation (cf. 2.6) of those results proves

$$\| \varphi_z \|_{\widetilde{H}^s(\Gamma)} \le \| \varphi_z \|_{L^2(\Gamma)}^{1-s} \| \varphi_z \|_{H_0^1(\Gamma)}^{s} \approx h_z^{1-s}. \qquad (5.7)$$

For the remaining proof of the reverse inequality we argue by duality,

$$\| \varphi_z \|_{\widetilde{H}^s(\Gamma)} = \sup_{\substack{\eta\in H^{-s}(\Gamma)\\ \eta\neq 0}} \frac{\langle \eta; \varphi_z \rangle}{\| \eta \|_{H^{-s}(\Gamma)}}. \qquad (5.8)$$

A lower bound of (5.8) is found by choosing a particular $\eta \in H_0^1(\Gamma)$ of the form

$$\eta = \varphi_z + \alpha\varphi_\zeta \tag{5.9}$$

where $\alpha \in \mathbb{R}$ and φ_ζ is another hat function. The corresponding node ζ is chosen as a neighbour, e.g., of second order, i.e., there exist $x \in \mathcal{N}$ with $x, z \in T$ and $x, \zeta \in T'$ for two elements $T, T' \in \mathcal{T}$. It is required that $\omega := \text{int}(\text{supp}\,\varphi_z \cup \text{supp}\,\varphi_\zeta)$ is open and connected. Note carefully that, in case there is no such node ζ, the mesh is too coarse, hence $h_z \approx \text{diam}\,(\Gamma)$ and so (5.6) degenerates to

$$1 \lesssim \| \varphi_z \|_{L^2(\Gamma)} \leq \| \varphi_z \|_{\widetilde{H}^s(\Gamma)} \leq \| \varphi_z \|_{H_0^1(\Gamma)} \lesssim 1.$$

Choose $\alpha := -\langle \varphi_z; 1\rangle / \langle \varphi_\zeta; 1\rangle$ in (5.9) and observe $|\alpha| \approx 1$. Then, $\langle \eta; 1\rangle = 0$ and

$$\|\eta\|_{\widetilde{H}^s(\Gamma)} \approx h_z^{1-s} \quad \text{for} \quad s = 0 \quad \text{or} \quad s = 1. \tag{5.10}$$

For any $\psi \in H_0^1(\Gamma)$, ω as above, and $\psi_\omega := \int_\omega \psi\, ds/|\omega|$ with surface area $|\omega|$, we have

$$\begin{aligned}\langle \eta; \psi\rangle = \langle \eta; \psi - \psi_\omega\rangle &\leq \| \eta \|_{L^2(\Gamma)} \| \psi - \psi_\omega \|_{L^2(\omega)} \\ &\lesssim h_z h_\omega \| \nabla\psi \|_{L^2(\omega)} \lesssim h_z^2 \| \psi \|_{H_0^1(\Gamma)}\end{aligned}$$

according to a Poincaré inequality on ω with diameter $h_\omega \approx h_z$. We conclude with interpolation of $H^{-s}(\Gamma) = [L^2(\Gamma); H^{-1}(\Gamma)]_s$ that

$$\begin{aligned}\| \eta \|_{H^{-s}(\Gamma)} \leq \| \eta \|_{L^2(\Gamma)}^{1-s} \| \eta \|_{H^{-1}(\Gamma)}^{s} &\approx h_z^{1-s} \sup_{\substack{\psi \in H_0^1(\Gamma) \\ \psi \neq 0}} \Big(\frac{\langle \eta; \psi\rangle}{\| \psi \|_{H_0^1(\Omega)}} \Big)^s \\ &\lesssim h_z^{1-s} h_z^{2s} = h_z^{1+s}. \end{aligned} \tag{5.11}$$

The combination of (5.8) and (5.11) with $\langle \eta; \varphi_z\rangle = \| \varphi_z \|_{L^2(\Gamma)}^2 \approx h_z^2$ leads to

$$\| \varphi_z \|_{H^{-s}(\Gamma)} \geq h_z^2 / h_z^{1+s} = h_z^{1-s}. \qquad \square$$

Remark 5.3. Using Lemma 5.3, a laborious direct calculation for [CMS, Theorem 5.1] can be shortened and generalized to all $0 \leq s \leq 1$. The crucial estimate therein requires $\langle V\chi; \chi\rangle \gtrsim h_\omega|\omega|$ for the single-layer potential operator applied to the characteristic function χ of ω (i.e., $\chi(x) = 1$ if $x \in \omega$ and $= 0$ otherwise). Taking a hat function φ with $\text{supp}\,\varphi \subset \omega$ and $\| \varphi \|_{L^2(\Gamma)} \approx h_\omega := \text{diam}\,(\omega)$, we find

$$\begin{aligned}\langle V\chi; \chi\rangle \approx \| \chi \|_{\widetilde{H}^{-1/2}(\Gamma)}^2 &\geq \sup_{\substack{\eta \in H^{1/2}(\Gamma) \\ \eta \neq 0}} \frac{\langle \chi; \eta\rangle^2}{\| \eta \|_{H^{1/2}(\Gamma)}^2} \geq \frac{\langle \chi; \varphi\rangle^2}{\| \varphi \|_{H^{1/2}(\Gamma)}^2} \\ &\approx \frac{|\omega|^2}{h_\omega} \approx h_\omega|\omega|. \qquad \square\end{aligned}$$

Proof of Theorem 5.2. We have $\| \varphi_z \|_W^2 \approx \| \varphi_z \|_{\widetilde{H}^{1/2}(\Gamma)}^2 \approx h_z$ owing to Lemma 5.3. A Cauchy inequality concludes the proof, namely,

$$\mu_z^2 \le \| R \|_{L^2(T_1 \cup T_2)}^2 \| \varphi_z \|_{L^2(T_1 \cup T_2)}^2 / h_z, \quad \text{whence}$$
$$\mu_z^2 \le h_z \| R \|_{L^2(T_1 \cup T_2)}^2. \qquad \square$$

6. Regularisation of the hypersingular integral

The evaluation of our refinement indicators $\eta_T := h^{1-s} \| R \|_{L^2(T)}$ requires an integration of $W\phi_h(x)$ over an element. This section is devoted to details on the computation of $W\phi_h(x)$ at a given point x on Γ in the three-dimensional situation. The evaluation of the hypersingular integral operator applied to a spline function

(6.1)
$$W\phi(x) = \frac{1}{2\pi} \; p.f. \int_\Gamma \frac{\partial}{\partial n_x} \frac{\partial}{\partial n_y} \frac{1}{|x-y|} \Big(\sum_{j=1}^n c_j \phi_j(y) \Big) \, dy \qquad \text{for } x \in \Gamma$$

can be decomposed into the computation of integrals on the mesh elements (*p.f.* denote the finite part or principle part of the integral [LS]). For triangles and linear base functions, we can evaluate the integrals analytically. On the reference triangle $T := \{(t_1, t_2) : 0 \le t_1 \le 1 - t_2 \le 1\}$ the part fini integrals are linear combinations of integrals $W_{k\ell}$.

Definition 6.1. *For $a, b, c \in \mathbb{R}^3$, $s_1, s_2 \in \mathbb{R}$ with $c = -s_1 a - s_2 b$, we define*

$$W_{k\ell}(a, b, c) = \; p.f. \int_0^1 \int_0^{1-t_1} \frac{t_1^k t_2^\ell}{|a t_1 + b t_2 + c|^3} \, dt_2 \, dt_1. \tag{6.2}$$

Theorem 6.1. *For $a, b \in \mathbb{R}^3$, $s_1, s_2 \in \mathbb{R}$, and $c := -s_1 a - s_2 b$, we have*

(6.3)
$$W_{00}(a, b, c) = -\frac{1}{|a \times b|^2} \left\{ \frac{|b + c|}{s_1(1 - s_1 - s_2)} + \frac{|c|}{s_1 s_2} + \frac{|a + c|}{s_2(1 - s_1 - s_2)} \right\}.$$

Proof. Let (s_1, s_2) be an interior point of T, $0 < s_1 < 1 - s_2 < 1$, and set

$$I_\varepsilon(a, b, c) := \int_{T \setminus B_\varepsilon(s_1, s_2)} \frac{1}{|a t_1 + b t_2 + c|^3} \, dt_2 \, dt_1 \quad \text{for} \quad \varepsilon > 0,$$

where $B_\varepsilon(s_1, s_2)$ denotes the ball around (s_1, s_2) with radius $\varepsilon > 0$. For $(t_1, t_2) \ne (s_1, s_2)$ there holds

$$\big((t_1 - s_1) \partial/\partial t_1 + (t_2 - s_2) \partial/\partial t_2 \big) |a t_1 + b t_2 + c|^{-3} = -3 |a t_1 + b t_2 + c|^{-3}.$$

Integration by parts with respect to t_1 and t_2 leads to

$$\begin{aligned}-3I_\varepsilon &= \int_{T\setminus B_\varepsilon(s_1,s_2)} \big((t_1-s_1)\partial/\partial t_1 \\ &\quad +(t_2-s_2)\partial/\partial t_2\big)|at_1+bt_2+c|^{-3}\,dt_2\,dt_1 \\ &= \int_{\partial(T\setminus B_\varepsilon(s_1,s_2))} \big((t_1-s_1)n_1(t_1,t_2) \\ &\quad +(t_2-s_2)n_2(t_1,t_2)\big)|at_1+bt_2+c|^{-3} - 2I_\varepsilon.\end{aligned}$$

The normal direction is oriented into the ball, i.e., we have the representation

$$\begin{aligned}&(t_1,t_2) = \varepsilon(\cos\varphi,\sin\varphi)+(s_1,s_2) \quad \text{and}\\ &(n_1,n_2) = -(\cos\varphi,\sin\varphi), \quad 0\le\varphi<2\pi.\end{aligned}$$

Therefore, we obtain

$$\begin{aligned}-I_\varepsilon &= \int_{\partial T}((t_1-s_1)n_1(t_1,t_2)+(t_2-s_2)n_2(t_1,t_2))|at_1+bt_2 \\ &\quad +c|^{-3}dt_1\,dt_2 - \int_0^{2\pi}(\varepsilon\cos\varphi(-\cos\varphi)+\varepsilon\sin\varphi(-\sin\varphi)) \\ &\quad \times|a\varepsilon\cos\varphi+b\varepsilon\sin\varphi|^{-3}\varepsilon\,d\varphi \\ &= s_2\int_0^1\frac{dt_1}{|at_1+c|^3}+(1-s_1-s_2)\int_0^1\frac{dt}{|(a-b)t+b+c|^3} \\ &\quad +s_1\int_0^1\frac{dt_2}{|bt_2+c|^3}+\frac{1}{\varepsilon}\int_0^{2\pi}|a\cos\varphi+b\sin\varphi|^{-3}\,d\varphi.\end{aligned}$$

Regularisation in the sense of Hadamard and simplification of the remaining integrals concludes the proof. The case $(s_1,s_2)\notin T$ is handled analogously by integration by parts without the regularisation. □

Theorem 6.2. *For $a,b\in\mathbb{R}^3$, $s_1,s_2\in\mathbb{R}$, and $c := s_1a-s_2b$, there are unique $q_1,q_2\in\mathbb{R}$ such that*

$$\begin{pmatrix}W_{10}(a,b,c)\\ W_{01}(a,b,c)\end{pmatrix} = -\frac{1}{|a\times b|^2}\begin{pmatrix}|b|^2 & -a\cdot b\\ -a\cdot b & |a|^2\end{pmatrix}\begin{pmatrix}q_1\\ q_2\end{pmatrix}+\begin{pmatrix}s_1\\ s_2\end{pmatrix}W_{00}(a,b,c).$$

These are given by $q_1 = I(a-b,b+c)-I(b,c)$ and $q_2 = I(a-b,b+c)-I(a,c)$ with

$$\begin{aligned}I(a,b) &:= \int_0^1|at+b|^{-1}\,dt \\ &= \frac{1}{|a|}\begin{cases}\operatorname{arsinh}\frac{a\cdot(a+b)}{|a\times b|}-\operatorname{arsinh}\frac{a\cdot b}{|a\times b|} & \text{if } |a\times b|>0,\\ \log\frac{a\cdot(a+b)}{a\cdot b} & \text{if } |a\times b|=0.\end{cases}\end{aligned}$$

Proof. We neglect the arguments (a, b, c) and define $\widetilde{W}_{10} := W_{10} - s_1 W_{00}$ and $\widetilde{W}_{01} := W_{01} - s_2 W_{00}$. Using the identities

$$-\frac{|a|^2(t_1 - s_1) + a \cdot b(t_2 - s_2)}{|a(t_1 - s_1) + b(t_2 - s_2)|^3} = \partial_{t_1} |a(t_1 - s_1) + b(t_2 - s_2)|^{-1},$$
$$-\frac{a \cdot b(t_1 - s_1) + |b|^2(t_2 - s_2)}{|a(t_1 - s_1) + b(t_2 - s_2)|^3} = \partial_{t_2} |a(t_1 - s_1) + b(t_2 - s_2)|^{-1},$$

we obtain a linear 2×2 system of equations

$$\begin{aligned} -|a|^2 \widetilde{W}_{10} - a \cdot b \widetilde{W}_{01} &= \int_0^1 \int_0^{1-t_1} \partial_{t_1} |a(t_1 - s_1) + b(t_2 - s_2)|^{-1} \, dt_2 \, dt_1 \\ &= q_1 \\ -a \cdot b \widetilde{W}_{10} - |b|^2 \widetilde{W}_{01} &= \int_0^1 \int_0^{1-t_1} \partial_{t_2} |a(t_1 - s_1) + b(t_2 - s_2)|^{-1} \, dt_2 \, dt_1 \\ &= q_2. \end{aligned}$$

The solution of which yields an identity for q_1, q_2, namely,

$$\begin{pmatrix} \widetilde{W}_{10} \\ \widetilde{W}_{01} \end{pmatrix} = -\frac{1}{|a \times b|^2} \begin{pmatrix} |b|^2 & -a \cdot b \\ -a \cdot b & |a|^2 \end{pmatrix} \begin{pmatrix} q_1 \\ q_2 \end{pmatrix} \tag{6.4}$$

An integration by parts in the inner integrals of q_1 and q_2 yields

$$\begin{aligned} q_1 &= \int_0^1 |(a - b)t_1 + b + c|^{-1} \, dt_1 - \int_0^1 |bt_2 + c|^{-1} \, dt_2 \\ &= I(a - b, b + c) - I(b, c), \\ q_2 &= \int_0^1 |(a - b)t_1 + b + c|^{-1} \, dt_1 - \int_0^1 |at_1 + c|^{-1} \, dt_1 \\ &= I(a - b, b + c) - I(a, c). \end{aligned} \tag{6.5}$$

□

With the above formulae for $\widetilde{W}_{jk}$, the point value of $W\phi$ for a hat function ϕ of Figure 1 is given by Formula (6.6) below. The important observation is that the hypersingular operator applied to a hat function on a planar domain only yields logarithmic singularities on element boundaries.

Theorem 6.3. *Let v be the common vertex point of the triangles $\Gamma_1, \ldots, \Gamma_n$, where $\Gamma_j = \{y = v + t_1 a_j + t_2 b_j : (t_1, t_2) \in T\}$, $j = 1, \ldots, n$. The edge vectors a_j, b_j are numbered such that $a_{j+1} = b_j$ and $a_{n+1} := a_1 = b_n$. For the hat function ϕ defined in the vertex v we obtain*

$$\begin{aligned} W\phi(x) = -\frac{1}{2\pi} \sum_{i=1}^{n} |a_i \times b_i| \Big(& \widetilde{W}_{01}(a_i, b_i, c) \\ & + \widetilde{W}_{10}(a_i, b_i, c) \Big) \quad \textit{with} \quad c = v - x. \end{aligned} \tag{6.6}$$

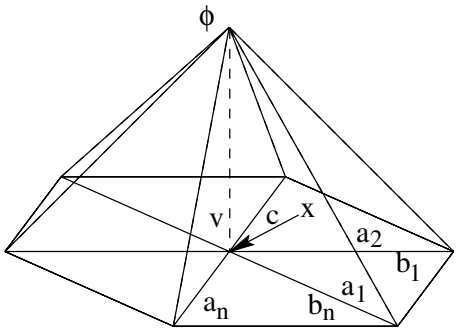

Fig. 1. Triangles supporting a hat function in Theorem 6.3

Proof. Introducing local coordinates and the unique representation $c = -s_{1,j}a_j - s_{2,j}b_j$ on the element Γ_j, we obtain

$$\begin{aligned} W\phi(x) &= \frac{1}{2\pi}\sum_{j=1}^{n}\int_0^1\int_0^{1-t_1}\frac{1-t_1-t_2}{|a_jt_1+b_jt_2+c|^3}\,dt_2\,dt_1 \\ &= \frac{1}{2\pi}\sum_{j=1}^{n}|a_j\times b_j|\Big((1-s_{1,j}-s_{2,j})W_{00}(a_j,b_j,c) \\ &\quad -\widetilde{W}_{01}(a_j,b_j,c)-\widetilde{W}_{10}(a_j,b_j,c)\Big). \end{aligned}$$

It remains to show that the first integral of the three in the last expression, namely

$$I := \sum_{j=1}^{n}|a_j\times b_j|(1-s_{1,j}-s_{2,j})W_{00}(a_j,b_j,c),$$

vanishes. With Theorem 6.1, $a_{j+1} = b_j$, and the relation

$$s_{1,j}|a_j\times b_j| = -s_{2,j+1}|a_{j+1}\times b_{j+1}|, \tag{6.7}$$

we can simplify

$$\begin{aligned} I &= -\sum_{j=1}^{n}\frac{1}{|a_j\times b_j|}\left(\frac{|b_j+c|}{s_{1,j}}+\frac{|c|(1-s_{1,j}-s_{2,j})}{s_{1,j}s_{2,j}}+\frac{|a_j+c|}{s_{2,j}}\right) \\ &= -\sum_{j=1}^{n}\frac{|b_j+c|-|c|}{|a_j\times b_j|s_{1,j}}-\sum_{j=1}^{n}\frac{|a_j+c|-|c|}{|a_j\times b_j|s_{2,j}}-\sum_{j=1}^{n}\frac{|c|}{|a_j\times b_j|s_{1,j}s_{2,j}} \end{aligned}$$

$$= \sum_{j=1}^{n} \frac{|a_{j+1}+c|-|c|}{|a_{j+1}\times b_{j+1}|s_{2,j+1}} - \sum_{j=1}^{n} \frac{|a_j+c|-|c|}{|a_j\times b_j|s_{2,j}} - \sum_{j=1}^{n} \frac{|c|}{|a_j\times b_j|s_{1,j}s_{2,j}}$$

$$= -\sum_{j=1}^{n} \frac{|c|}{|a_j\times b_j|s_{1,j}s_{2,j}}.$$

For a_j, b_j, c in the same plane, we have

$$\frac{1}{s_{1,j}s_{2,j}} = -\frac{1}{|c|^2}\left(\frac{cb_j}{s_{1,j}} + \frac{ca_j}{s_{2,j}}\right).$$

Therefore we obtain with (6.7)

$$I = \frac{1}{|c|}\sum_{j=1}^{n} \frac{cb_j}{|a_j\times b_j|s_{1,j}} + \frac{1}{|c|}\sum_{j=1}^{n} \frac{ca_j}{|a_j\times b_j|s_{2,j}}$$

$$= \frac{1}{|c|}\sum_{j=1}^{n} \frac{-ca_{j+1}}{|a_{j+1}\times b_{j+1}|s_{2,j+1}} + \frac{1}{|c|}\sum_{j=1}^{n} \frac{ca_j}{|a_j\times b_j|s_{2,j}} = 0.\square$$

7 Numerical results

This section is devoted to the presentation and discussion of two numerical experiments. In all examples, the flat boundary Γ is partitioned by a regular triangulation into triangles (and, for comparison, into rectangles in two experiments of Example 7.2). With basis functions $(\varphi_z : z \in \mathcal{K})$, the discrete problem addresses a linear system of equations with a stiffness matrix,

$$\begin{aligned} \langle W\varphi_z; \varphi_\zeta\rangle &= \langle V\nabla_\Gamma\varphi_z; \nabla_\Gamma\varphi_\zeta\rangle \\ &:= \langle V\,\partial\varphi_z/\partial x; \partial\varphi_\zeta/\partial x\rangle + \langle V\,\partial\varphi_z/\partial y; \partial\varphi_\zeta/\partial y\rangle \quad \text{for } z,\zeta\in\mathcal{K}. \end{aligned} \tag{7.1}$$

Here the single layer potential V is applied to the two components of the surface gradients of φ_z and φ_ζ [N]. Then, the entry $\langle W\varphi_z; \varphi_\zeta\rangle$ can be calculated analytically [M2] as well as, for piecewise affine g, the entry $\langle g; \varphi_z\rangle$ of the right-hand side. The discrete system is solved exactly [M1].

Algorithm ($\boldsymbol{A_R}$) resp. ($\boldsymbol{A_H}$).

(a) Start with $k = 0$ and a coarse triangulation $\mathcal{T}_0$.
(b) Compute stiffness matrix $A = (\langle W\varphi_z; \varphi_\zeta\rangle : z, \zeta \in \mathcal{K}_k)$, right-hand side b, and discrete solution u_N (the index N indicates the number of degrees of freedom), $u_N = \sum_{z\in\mathcal{K}_k} x_z\varphi_z$, of the discrete problem $Ax = b$ with respect to the current mesh $\mathcal{T}_k$ with $N = \mathrm{card}(\mathcal{K}_k)$ degrees of freedom and free nodes $\mathcal{K}_k$.

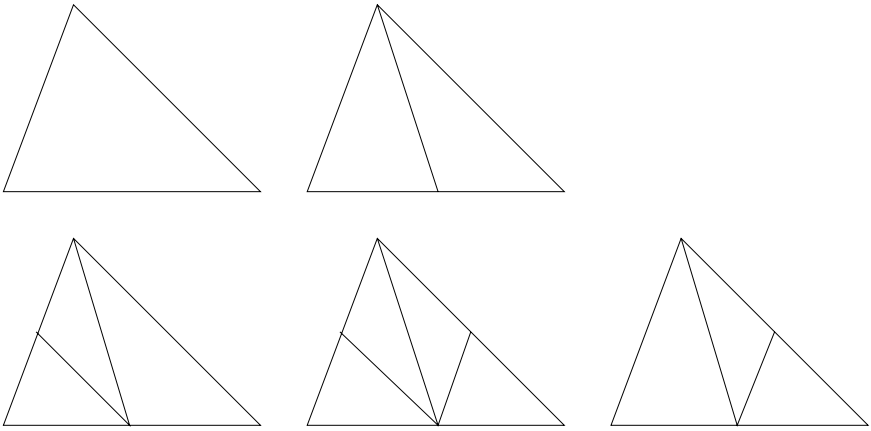

Fig. 2. Possible refinements (a), (b) on top and (c), (d), (e) below in Algorithm (A_R)) resp. (A_H) with respect to the longest edge in a triangle

(c) Display the error $E_N := \| u - u_N \|_W = \left(\| u \|_W^2 - \| u_N \|_W^2 \right)^{1/2}$ and estimators

$$\eta_N := \| h_T^{1/2} R \|_{L^2(\Gamma)} \qquad \text{for the residual } R := f - W u_N,$$
$$\mu_N := \Big(\sum_{z \in \mathcal{K}_h \setminus \mathcal{K}_k} \mu_z^2 \Big)^{1/2} \qquad \text{from (5.4)}$$

for the current coarse mesh $\mathcal{T}_H = \mathcal{T}_k$ and one (fictitious) refinement $\mathcal{T}_h$ with new nodes $\mathcal{K}_h \setminus \mathcal{K}_k$ on all edges.

(d) Decide to terminate or to continue with (e) based on η_N resp. μ_N.

(e) Given a parameter $0 \le \theta \le 1$, mark $(1 - \theta)$ card$(\mathcal{T}_k)$ elements for refinement by choosing a corresponding level $\tau > 0$. Then, mark $T \in \mathcal{T}_k$ provided

$$\eta_T \ge \tau,$$

where $\eta_{T'}$ for $T \in \mathcal{T}_k$ denotes the local refinement indicator

$$\eta_T := h_T^{1/2} \| R \|_{L^2(T)} \quad \text{for } (A_R) \quad \text{resp.}$$
$$\eta_T := \Big(\sum_{\substack{z \in T \\ z \in \mathcal{K}_h \setminus \mathcal{K}_k}} \mu_z^2 \Big)^{1/2} \quad \text{for } (A_H).$$

(f) Refine each marked element into 4 new elements as shown in Figure 2(d). Further, refine neighbouring elements to avoid hanging notes and so design a new mesh $\mathcal{T}_{k+1}$, update k, and go to (b).

Remarks 7.1. (i) Algorithm (A_R) resp. (A_H) generated all the meshes and corresponding results reported below. (The simplified termination criterion in (d) was based on individual limits for N).

(ii) For $\theta = 0$, Algorithm (A_R) and (A_H) generate a uniform refinement while, e.g., $\theta = 0.8$, in the examples below yield effectively adapted meshes.

(iii) The value $\| u \|_W$ in (c) was independently computed by extrapolation of discrete approximations for a sequence of uniformly refined meshes.

(iv) The crucial calculation of η_T in (c) utilizes the representation of Theorem 6.3 to evaluate $(W\varphi_z)(x)$ for a hat function φ_z and a point x. As this integration involved only logarithmic singularities, we computed $R(x)$ by a 4×4 quadrature formula as follows: Duffy's transformation

$$\Psi_1(\xi_1, \xi_2) := (\xi_1, (1 - \xi_1)\xi_2)$$

maps the unit square $[0, 1]^2$ onto the reference triangle

$$\{(x, y) \in \mathbb{R}^2 \,:\, 0 \le x, y \le 1, 0 \le x + y \le 1\}.$$

Then, a standard affine transformation Ψ_2 maps the reference triangle onto T by a standard affine map. We computed

$$\int_T |R|^2 \, dT = \int_0^1 \int_0^1 (R \circ \Psi_2 \circ \Psi_1)^2 \, |\det D(\Psi_2 \circ \Psi_1)| \, dx \, dy$$

by a standard 4×4 tensor product Gaussian quadrature rule on $[0, 1]^2$.

(v) For the calculation of $\mu_z = \langle R; \varphi_z \rangle / \| \varphi_z \|_W$, $\| \varphi_z \|_W$ can be calculated as described for the stiffness matrix at the beginning of this section. The fictitious mesh $\mathcal{T}_h$ is a uniform refinement where any edge is halved (cf. Figure 2.(d)). Note that R is the known residual and no further discrete problem needs to be solved.

(vi) The mesh refinement (as in Figure 2.(c), (d), or (e)) may be necessary if a neighbouring element with a corresponding longest edge is marked.

(vii) The tolerance τ in (e) is defined by

$$\tau := \max \left\{ t \ge 0 \,:\, (1 - \theta) \operatorname{card}(\mathcal{T}_k) \le \operatorname{card}(\{T \in \mathcal{T}_k \,:\, \eta_T \ge t\}) \right\}.$$

Marking $(1 - \theta) \operatorname{card}(\mathcal{T}_k)$ elements for refinement, we expect the new mesh $\mathcal{T}_{k+1}$ to consist of at least $\theta \operatorname{card}(\mathcal{T}_k) + 4(1 - \theta) \operatorname{card}(\mathcal{T}_k) = (4 - 3\theta) \operatorname{card}(\mathcal{T}_k)$ elements. Hence, $(4 - 3\theta)$ is the factor by which the number of elements is aimed to be raised. Since neighbouring elements are possibly refined in (f) we obtain $\operatorname{card}(\mathcal{T}_{k+1}) \ge (4 - 3\theta) \operatorname{card}(\mathcal{T}_k)$.

(viii) In the context of adaptive finite element methods for partial differential equations, it can be shown that an algorithm analogous to Algorithm (A) converges linearly [D, DN]. This is an open question in the context of integral equations.

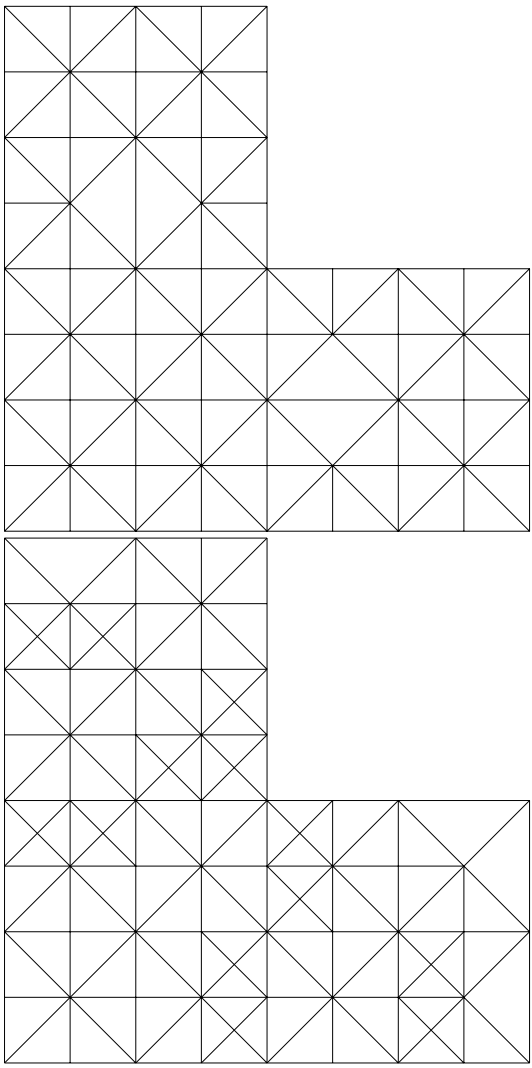

Fig. 3. Mesh $\mathcal{T}_3$ generated by Algorithm (A_R) (left) and (A_H) (right) for $\theta = 0.8$ in Example 7.1

7.1 Example on L-shaped screen

A typical example for screen problems is the Neumann problem of the Laplacian with boundary data $g(x) = 1$ on the L-shaped screen Γ, shown in Figures 3, 4, and 5. The initial mesh $\mathcal{T}_0$ with $N = 5$ degrees of freedom consisted of 24 triangles obtained from a partition of Γ into 12 squares of size $1/2$ which are halved along the main diagonal. We first run the algorithm for uniform refinement ($\theta = 0$) with the empirical value $\| u \|_W = 1.4310$ in

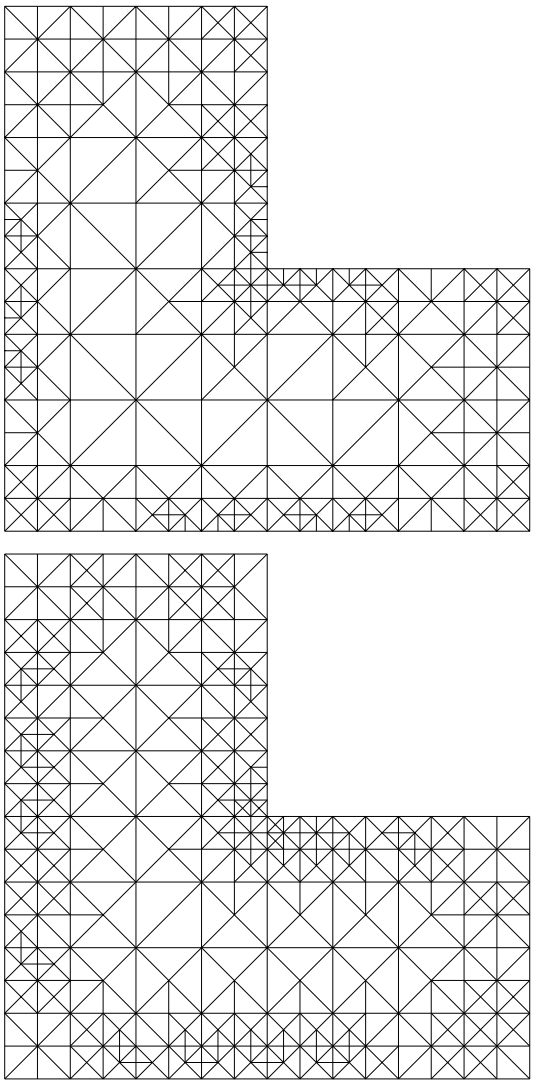

Fig. 4. Mesh $\mathcal{T}_5$ generated by Algorithm (A_R) (left) and (A_H) (right) for $\theta = 0.8$ in Example 7.1

step (d). The outcome N, E_N, η_N, μ_N is displayed in Table 1 together with the cpu-times t_{mat}, t_η, t_μ (in seconds) and the experimental convergence rate

$$\alpha_N := \log(E_{N'}/E_N) \;/\; \log(N/N')$$

Here, N' and $E_{N'}$ are the corresponding values of the previous step based on $\mathcal{T}_{k-1}$. Notice that $\alpha = 1/2$ indicates linear convergence in terms of a fictitious mesh size $h = 1/\sqrt{N}$. Instead of linear convergence ($\alpha = 1/2$), Table 1

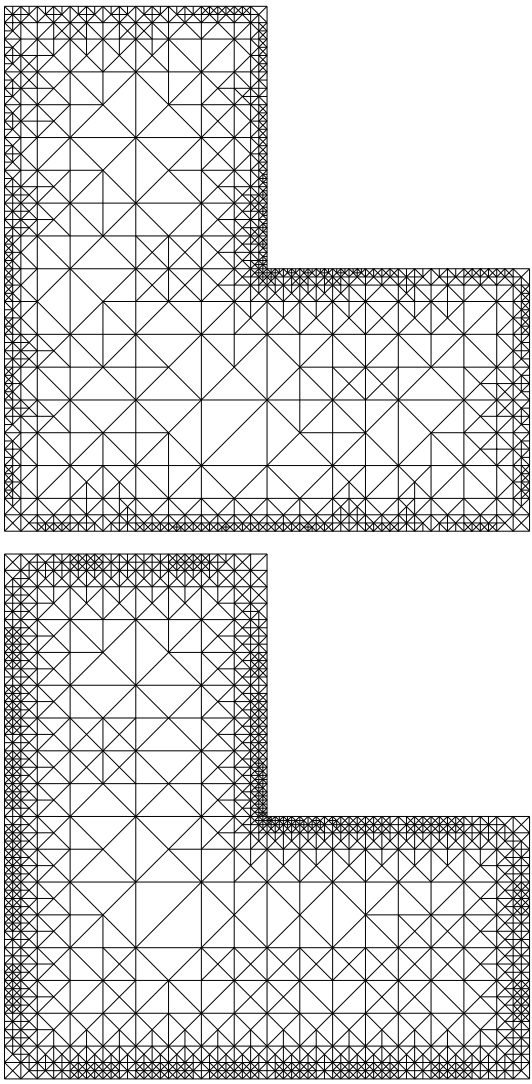

Fig. 5. Mesh $\mathcal{T}_7$ generated by Algorithm (A_R) (left) and (A_H) (right) for $\theta = 0.8$ in Example 7.1

shows $\alpha \approx 1/4$, which corresponds to $O(h^{1/2})$. This is expected owing to the edge singularities along the screen boundary.

The time (in seconds) for computing the Galerkin matrix is denoted by t_{mat}, and the times for computing the two error indicators are given by t_η, t_μ. The computations have been done using an Intel(R) Xeon(TM) CPU with 2.80 GHz and 4 GByte of memory. Note, that there holds $t_\mu \approx 8t_{\text{mat}}$. The hierachical error indicator is obtained by computing the residual on a refined

Table 1. Numerical results for uniform mesh refinement in Example 7.1

N	E_N	η_N	μ_N	E_N/η_N	E_N/μ_N	α_N	t_{mat}	t_η	t_μ
33	0.5794817	0.9423710	0.3471134	0.61492	1.66943		0.06000	0.44000	0.50000
161	0.3925993	0.6596814	0.2419290	0.59513	1.62279	0.246	0.98000	7.00000	7.50000
705	0.2708639	0.4609843	0.1681837	0.58758	1.61052	0.251	15.6400	111.660	117.900
2945	0.1884173	0.3236354	0.1172190	0.58219	1.60740	0.254	251.350	1811.83	1875.76
12033	0.1317638	0.2279023	0.0820724	0.57816	1.60546	0.254	4035.66	28780.0	30030.0

Table 2. Output of Algorithm (A_R) for $\theta = 0.8$ in Example 7.1

N	E_N	η_N	μ_N	E_N/η_N	E_N/μ_N	α_N	t_{mat}	t_η	t_μ
12	0.6968136	1.2371191	0.4427737	0.56326	1.57375		0.02000	0.10000	0.12000
31	0.5816609	0.9437129	0.3463353	0.61635	1.67947	0.190	0.05000	0.39000	0.49000
70	0.4503962	0.7735382	0.2905099	0.58225	1.55036	0.314	0.23000	1.63000	1.86000
163	0.3180149	0.5879044	0.2145841	0.54093	1.48201	0.412	1.07000	7.52000	8.39000
360	0.2190819	0.4412660	0.1630947	0.49648	1.34328	0.470	4.88000	34.2300	37.6000
762	0.1474977	0.3260425	0.1225931	0.45239	1.20315	0.528	20.9800	149.380	162.000
1598	0.0986230	0.2391711	0.0916457	0.41235	1.07613	0.544	90.6400	643.510	695.710
3393	0.0871337	0.1741430	0.0672880	0.50036	1.29494	0.164	400.530	2854.65	3060.09
7146	0.0485286	0.1287967	0.0504777	0.37678	0.96139	0.786	1755.40	12500.0	13350.0

Table 3. Output of Algorithm (A_H) for $\theta = 0.8$ in Example 7.1

N	E_N	η_N	μ_N	E_N/η_N	E_N/μ_N	α_N	t_{mat}	t_η	t_μ
20	0.6448391	1.1641380	0.4062413	0.55392	1.58733		0.02000	0.17000	0.22000
46	0.5538872	0.9256691	0.3360857	0.59836	1.64805	0.183	0.09000	0.68000	0.81000
115	0.4116299	0.7580858	0.2512338	0.54299	1.63843	0.324	0.48000	3.35000	3.89000
250	0.3187360	0.5808173	0.2035831	0.54877	1.56563	0.329	2.18000	14.9500	17.1500
532	0.2184784	0.4308609	0.1542260	0.50707	1.41661	0.500	9.60000	65.8500	75.0100
1161	0.1489778	0.3192171	0.1157990	0.46670	1.28652	0.491	44.8300	307.610	348.270
2478	0.0986286	0.2313451	0.0850653	0.42633	1.15945	0.544	202.030	1388.87	1558.08
5287	0.0843851	0.1685591	0.0628799	0.50063	1.34200	0.206	909.570	6192.60	6965.31

grid containing four times as many elements as before, and the Galerkin matrix is obtained by taking into account the symmetry, i.e., we need only half of the time. Together this gives a factor of 8.

To improve the accuracy effectively, we run Algorithm (A_R) and (A_H) for $\theta = 0.8$. The errors and error estimators are displayed in Table 2 and 3, the resulting meshes $\mathcal{T}_3$, $\mathcal{T}_5$, and $\mathcal{T}_7$ are shown in Figure 3, 4, and 5. For both algorithms, we observe a high refinement towards the edges of Γ, a moderate refinement near the re-entering corner, and little refinements on the other (convex) corners of Γ. The resulting experimental convergence rates are improved to values around $1/2$ which indicates linear convergence. This improvement is in agreement with our expectation as the three-dimensional edge singularities dominate over corner singularities on the surface.

In Table 1, 2, and 3, the value E_N/η_N stays bounded from above in agreement with our reliability bound $E_N \leq C\eta_N$. The values are bounded from below as well which provides empirical evidence of efficiency. The same observation applies to the hierarchical error estimator which is always

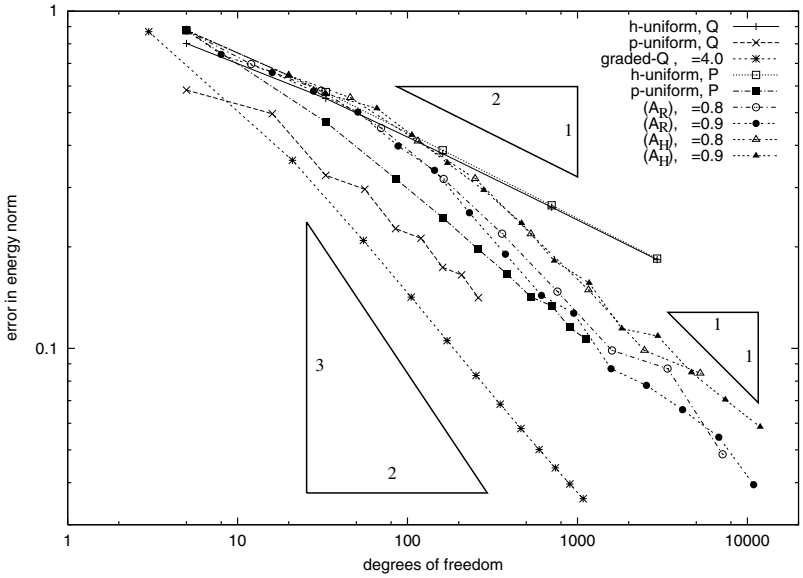

Fig. 6. Neumann problem on the L-shape in Example 7.1

efficient (c.f. Remark 5.2 (ii)). Theoretically, its reliability is guaranteed under the saturation assumption (5.2) to hold.

Further numerical experiments and comparisons are compactly displayed in Fig. 6, where we plotted the energy error E_N versus the number of degrees of freedom N. Both axis are scaled logarithmically. Related entries are plotted with the same symbol (e.g., $\circ$, $+$, $\times$) and linked by (e.g., full, dashed, dotted) straight lines.

Algorithm (A_R) and (A_H) run for $\theta = 0.9$ as well. In comparison with the output for $\theta = 0.8$ (already shown in Table 2 and 3) and $\theta = 0$ (already shown in Table 1) only little further improvement is observed. Since a larger value of θ results in a larger number of refinement levels, it appears doubtful that $\theta = 0.9$ is a better choice. However, even with a larger parameter θ, the convergence rate remains linearly. For comparison, Figure 6 shows numerical results for Q_1 finite elements as well. To avoid hanging nodes, a tensor product grid is employed. Besides a uniform mesh refinement (labelled *h-uniform* Q_1) we run a graded tensor product mesh with distance $(j/N)^4$, for $j = 1, \ldots, N$, from the boundary edge near to the corner points of Γ. Figure 6 displays the best performance for the graded strategy with linear convergence. Further experiments for a uniform grid of rectangles resp. triangles with the p-version show no further improvement of the experimental convergence rate.

7.2 Example on the unit square screen

Our second example illustrates the interaction of a singular right-hand side with edge singularities on the square $\Gamma = [-1, 1]^2$ shown in Figures 7, 8, and 9. The boundary data $g(x) = 1/|x - (0, 1.01)|$ has a singularity at one point $(0, 1.01)$ near the edge of Γ. The initial mesh $\mathcal{T}_0$ with $N = 9$ degrees of freedom consisted of 32 triangles. It was obtained by a partition of the unit square into 16 squares which were halved along the main diagonal. The numerical evaluation of the right-hand side is performed by the quadrature rule from Remark 7.1.(iv) based on a 2×2 Gaussian quadrature rule.

We first run the algorithm with uniform mesh refinement, i.e., $\theta = 0$. We used the extrapolated energy norm $\| u \|_W = 2.511$ in step (c) of the algorithm. The numerical results are shown in Table 4 with an experimental convergence rate $\alpha \approx 1/4$. To improve this rate, we run Algorithm (A_R) and (A_H) with $\theta = 0.8$. The errors and error estimators are shown in Table 5 and Table 6, the corresponding meshed in Figures 7, 8, and 9. The refinement towards the singular point is much higher than the usual refinement towards the edges. The resulting experimental convergence rates are very much improved to almost linear convergence. The error estimators η_N and μ_N behave efficient and reliable in this example.

In addition to the described adaptive schemes on triangles, Figure 10 displays uniform h- and p-version on rectangles and further a graded mesh version on rectangles.

7.3 Concluding remarks

(i) The examples clearly validate the reliability of the estimator η_N and the efficiency of μ_N. Moreover, they provide strong numerical evidence for the efficiency of η_N and the reliability of μ_N.

(ii) The numerical experiments clearly illustrate the superiority of automatic adaptive over uniform mesh-refinements in the presence of edge-singularities. The optimally graded version, however, performs slightly better.

(iii) An experimental convergence rate higher than linear convergence is not observed in our examples, although two-dimensional calculations result in an expected convergence rate $3/2$. Our interpretation is that conforming triangles require too much degrees of freedom to resolve an anisotropic layer structure as they refine isotropically. A comparison on isotropic vs. anisotropic refinement is possible with numerical results in [CMS] for Symm's integral equation with the related single layer potential V (cf. (7.1) for a link of V and W). The experiments in [CMS] with rectangles of high and low aspect ratios show that indeed a speed-up of a factor $3/2$ in the convergence rate is possible.

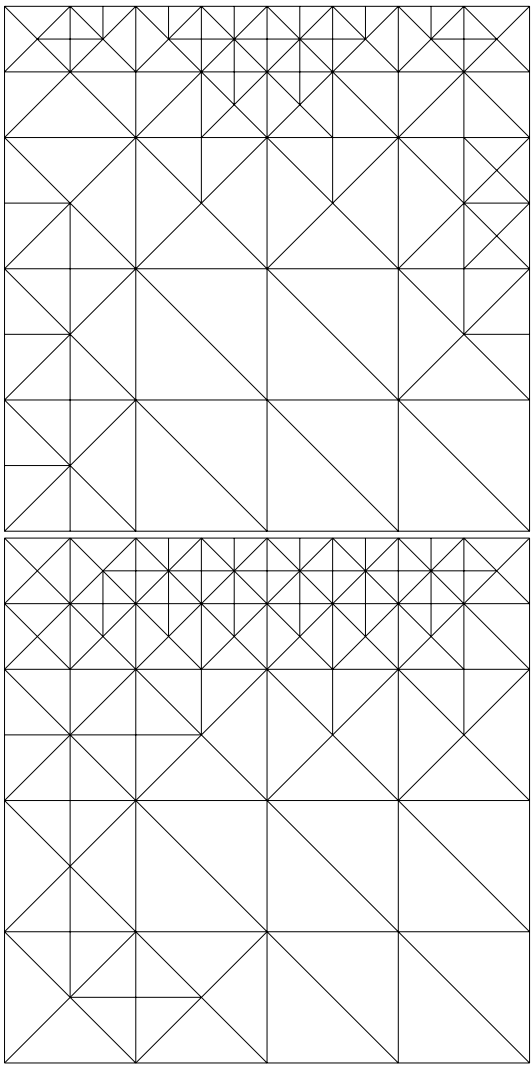

Fig. 7. Mesh $\mathcal{T}_3$ generated by (A_R) (left) and (A_H) (right) for $\theta = 0.8$ in Example 7.2

(iv) The optimal grading parameter is $\beta = 3 + \varepsilon$ and we chose $\beta = 4$ in the experiments. We refer to the literature for proofs and details on graded meshes [PS, P].

(v) The following heuristic arguments illustrate why we should expect linear convergence at most when we pass from anisotropic to isotropic refinements. Given an anisotropic triangulation $\mathcal{T}$ graded towards the edges there are at least $O(1/H)$ elements with a length H and a width H^β in $\mathcal{T}$; H denotes the maximal mesh-size in $\mathcal{T}$ and β is the grading parameter [PS, P]. A corresponding isotropic triangulation $\mathcal{T}^{(\text{isotropic})}$

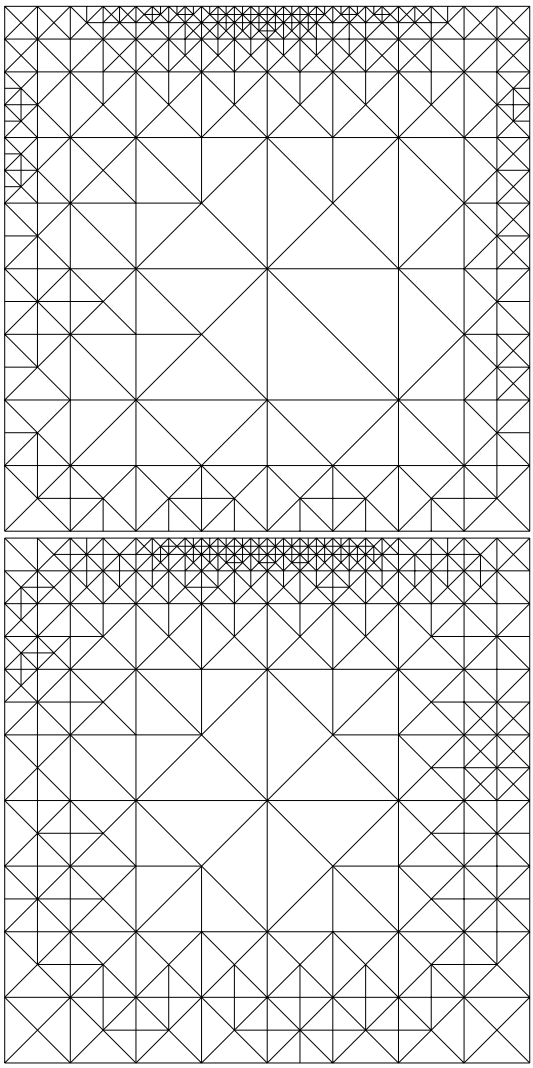

Fig. 8. Mesh $\mathcal{T}_5$ generated by (A_R) (left) and (A_H) (right) for $\theta = 0.8$ in Example 7.2

requires elements along the edges of the same width H^β to result in the same accuracy. The length of those elements, however, is of the same order $O(H^\beta)$ to limit the aspect ratio. Thus, $\mathcal{T}^{(\text{isotropic})}$ needs more elements for the same accuracy. If there are $N \propto H^{-2}$ elements in the graded mesh $\mathcal{T}$ we have more than $N^{(\text{isotropic})} \propto H^{-\beta}$ in $\mathcal{T}^{(\text{isotropic})}$. Since $\mathcal{T}$ yields the optimal convergence rate 3/2 (for P_1 or Q_1 finite elements) in terms of mesh-sizes, we have

$$3/4 = \log(E_N/E_0) \;/\; \log(N_0/N).$$

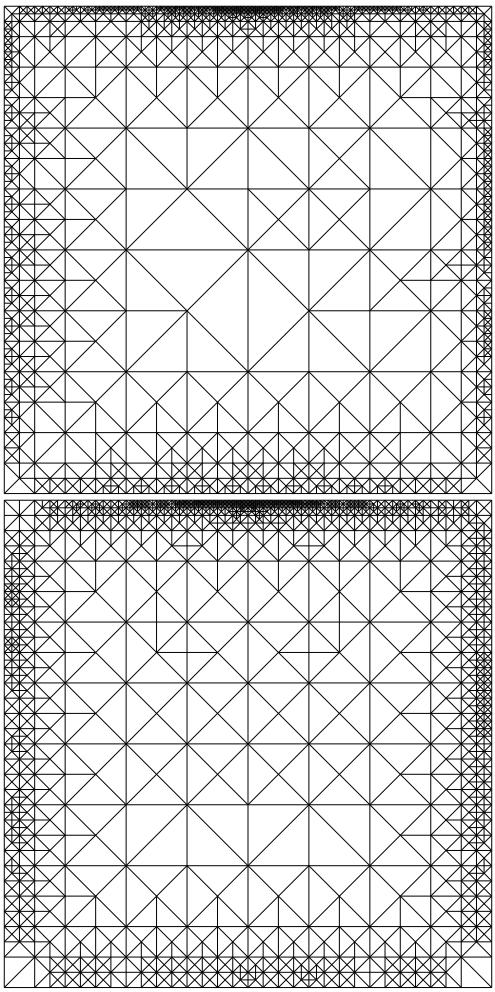

Fig. 9. Mesh $\mathcal{T}_7$ generated by (A_R) (left) and (A_H) (right) for $\theta = 0.8$ in Example 7.2

Table 4. Numerical results for uniform mesh refinement in Example 7.2

N	E_N	η_N	μ_N	E_N/η_N	E_N/μ_N	α_N	t_{mat}	t_η	t_μ
49	1.1439843	2.1480329	0.7094919	0.53257	1.61240		0.11000	0.77000	0.87000
225	0.8340395	1.5157682	0.5289063	0.55024	1.57691	0.207	1.79000	12.1800	13.3100
961	0.5947405	1.0548148	0.3807662	0.56383	1.56196	0.233	28.7200	196.550	209.350
3969	0.4184993	0.7322123	0.2669809	0.57155	1.56753	0.248	461.760	3203.61	3340.04

For the isotropic mesh $\mathcal{T}^{(\text{isotropic})}$ we assume the same error $E_N^{(\text{isotropic})} = E_N$ but the larger number $N^{(\text{isotropic})} \propto H^{-\beta} \propto N^{\beta/2}$ of degrees of freedom. This leads to an experimental convergence rate

Table 5. Output of Algorithm (A_R) for $\theta = 0.8$ in Example 7.2

N	E_N	η_N	μ_N	E_N/η_N	E_N/μ_N	α_N	t_{mat}	t_η	t_μ
22	1.2072099	2.2541222	0.7637518	0.53556	1.58063		0.02000	0.19000	0.24000
48	0.9097344	1.6535456	0.5842659	0.55017	1.55706	0.363	0.11000	0.77000	0.92000
104	0.6769054	1.2157873	0.4378091	0.55676	1.54612	0.382	0.46000	3.09000	3.58000
213	0.4911718	0.8713807	0.3197725	0.56367	1.53600	0.447	1.82000	12.5000	14.2200
445	0.3587789	0.6317357	0.2324232	0.56793	1.54364	0.426	7.56000	51.8100	58.9200
922	0.2604540	0.4540298	0.1672535	0.57365	1.55724	0.440	31.8900	217.630	246.270
1892	0.1915644	0.3250785	0.1202900	0.58929	1.59252	0.427	133.260	912.130	1023.62
3863	0.1439960	0.2320993	0.0860914	0.62041	1.67260	0.400	551.970	3784.22	4224.97
7915	0.1123453	0.1656719	0.0616006	0.67812	1.82377	0.346	2297.34	15710.0	17600.0

Table 6. Output of Algorithm (A_H) for $\theta = 0.8$ in Example 7.2

N	E_N	η_N	μ_N	E_N/η_N	E_N/μ_N	α_N	t_{mat}	t_η	t_μ
27	1.1759280	2.2276479	0.7304770	0.52788	1.60981		0.03000	0.25000	0.30000
58	0.8963254	1.6612351	0.5637360	0.53955	1.58997	0.355	0.14000	0.94000	1.12000
131	0.6644998	1.2212580	0.4228734	0.54411	1.57139	0.367	0.63000	4.26000	4.92000
268	0.4942562	0.8997397	0.3157851	0.54933	1.56517	0.414	2.49000	17.0800	19.4400
565	0.3611764	0.6547454	0.2295822	0.55163	1.57319	0.421	10.7500	73.6800	83.2800
1152	0.2655666	0.4726521	0.1677682	0.56186	1.58294	0.432	44.2600	301.630	340.740
2325	0.1955947	0.3383994	0.1210463	0.57800	1.61587	0.436	179.660	1234.14	1376.86
4711	0.1471338	0.2424768	0.0869671	0.60680	1.69183	0.403	735.370	5020.11	5607.81
9482	0.1146502	0.1733238	0.0625805	0.66148	1.83204	0.357	2975.56	20360.0	22710.0

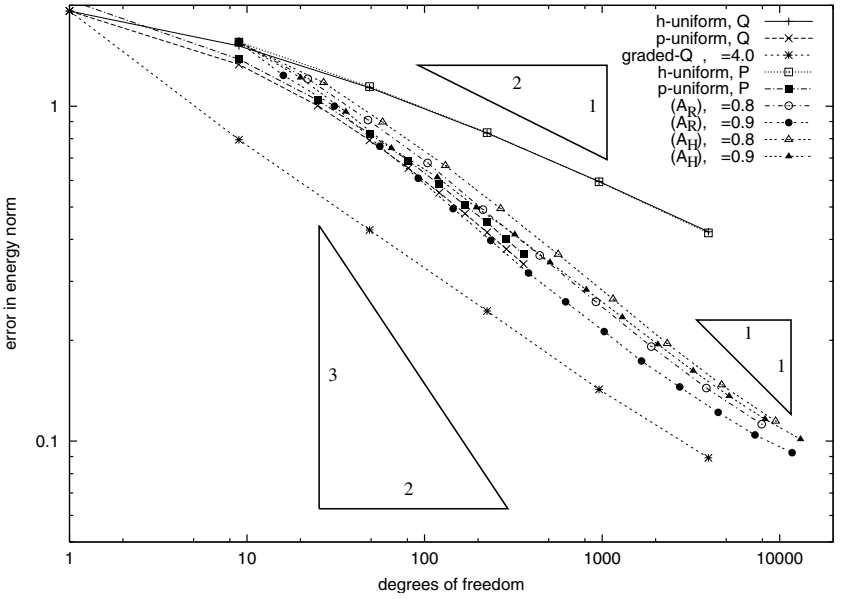

Fig. 10. Neumann problem on the unit square in Example 7.2

$$\alpha^{(\text{isotropic})} = \frac{\log(E_N^{(\text{isotropic})}/E_0)}{\log(N_0/N^{(\text{isotropic})})} = \frac{3}{4}\,\frac{\log(N_0/N)}{\log(N_0/N^{\beta/2})} = \frac{3}{4}\,\frac{1-\log(N_0)/\log(N)}{\beta/2-\log(N_0)/\log(N)}.$$

For $N^{(\text{isotropic})} = N^{\beta/2}$, this tends to $3/(2\beta) \le 1/2$ as $N \to \infty$. Although this estimate is very optimistic, the experimental convergence rates up to $1/2$ are indeed seen in the two experiments of this section.

(vi) The adaptive design of anisotropic triangular meshes is a subtle question for finite element methods even for partial differential equations (as the aspect ratio affects the a posteriori estimates). Our discussion shows, however, that anisotropic elements are unambiguously needed.

Acknowledgements. Parts of this paper were written while the first author (CC) enjoyed the hospitability of the Max Planck Institute for Mathematics in the Sciences (MIS) in Leipzig, Germany, whose support is thankfully acknowledged. The third author (DPr) acknowledges support through the DFG-Graduiertenkolleg 357 *Effiziente Algorithmen und Mehrskalenmethoden* at Christian-Albrechts-Universität zu Kiel, Germany.

References

[BL] Bergh, J., Löfström, J.: Interpolation spaces. Vol. **223** of Grundlehren der mathematischen Wissenschaften, Springer Verlag, Berlin, 1976

[C1] Carstensen, C.: Efficiency of a posteriori BEM error estimates for first kind integral equations on quasi-uniform meshes. Math. Comp. **65**, 69–84 (1996)

[C2] Carstensen, C.: An a posteriori error estimate for a first-kind integral equation. Math. Comp. **66**, 139–155 (1997)

[CB] Carstensen, C., Bartels, S.: Each averaging technique yields reliable a posteriori error control in FEM on unstructured grids, Part I: Low order conforming, nonconforming, and mixed FEM. Math. Comp. **71**, 945–969 (2002)

[CMS] Carstensen, C., Maischak, M., Stephan, E.P.: A posteriori error estimate and h-adaptive algorithm on surfaces for Symm's integral equation. Numer. Math. **90**, 197–213 (2001)

[CS] Carstensen, C., Stephan, E.P.: A posteriori error estimates for boundary element methods. Math. Comp. **64**, 483–500 (1995)

[D] Doerfler, W.: A convergent adaptive algorithm for Poisson's equation. SIAM J. Numer. Anal. **33**(3), 1106–1124 (1996)

[DN] Doerfler, W., Nochetto, R.H.: Small data oscillation implies the saturation assumption. Numer. Math. **91**, 1–12 (2002)

[L] McLean, W.: Strongly elliptic systems and boundary integral equations. Cambridge, 2000

[LS] Lage, C., Sauter, S.A.: Transformation of hypersingular integrals and black-box cubature. Math. Comp. **70**, 223–250 (2001)

[M1] Maischak, M.: Manual of the software package maiprogs. Technical report **ifam48**. Institut für Angewandte Mathematik, Universität Hannover, Hannover 2001 (`ftp://ftp.ifam.uni-hannover.de/pub/preprints/ifam48.ps.Z`)

[M2] Maischak, M.: Analytical evaluation of potentials and computation of Galerkin integrals on triangles and parallelograms. Technical report **ifam50**, Institut für Angewandte Mathematik, Universität Hannover, Hannover 2001 (`ftp://ftp.ifam.uni-hannover.de/pub/preprints/ifam50.ps.Z`)

[MaS] Maischak, M., Stephan, E.P.: A hierarchical error estimator for hypersingular integral equations in $\mathbb{R}^3$ on triangular meshes. In preparation

[MuS] Mund, P., Stephan, E.P.: An adaptive two-level method for hypersingular integral equations in $\mathbb{R}^3$. ANZIAM J. **42**, 1019–1033 (2000)

[N] Nedelec, J.C.: Integral equations with nonintegrable kernels. Int. Eqs. Oper. Theor. **5**, 562–572 (1982)

[P] von Petersdorff, T.: Randwertprobleme der Elastizitätstheorie für Polyeder – Singularitäten und Approximation mit Randelementmethoden. PhD thesis, Darmstadt, 1989

[PS] von Petersdorff, T., Stephan, E.P.: Regularity of mixed boundary value problems in $\mathbb{R}^3$ and boundary element methods on graded meshes. Math. Meth. Appl. Sci. **12**, 229–249 (1990)

[SS] Stephan, E.P., Suri, M.: The h-p version of the boundary element method on polygonal domains with quasiuniform meshes. RAIRO Analy. Numer. **25**(6), 783–807 (1991)